

TCAD simulation and radiation damage modeling for low gain avalanche detector

Tao Yang, Kewei Wu, Mei Zhao, Xuewei Jia, Yuhang Tan, Suyu Xiao, Kai Liu, Mengzhao Li, Yunyun Fan, Shuqi Li, Chengjun Yu, Han Cui, Hao Zeng, Mingjie Zhai, Shuiting Xin, Maoqiang Jing, Zhijun Liang, João Guimarães da Costa, Gangping Yan, Qionghua Zhai, Mingzheng Ding, Gaobo Xu, Huaxiang Yin, Gregor Kramberger, and Xin Shi

Abstract—We report a precise TCAD simulation for low gain avalanche detector (LGAD) with calibration by secondary ion mass spectroscopy (SIMS). The radiation model - LGAD Radiation Damage Model (LRDM) combines local acceptor degeneration with global deep energy levels is proposed. The LRDM could predict the leakage current level and the behavior of capacitance for irradiated LGAD sensor at -30 °C after irradiation fluence $\Phi_{\text{eq}} = 2.5 \times 10^{15} \text{ n}_{\text{eq}}/\text{cm}^2$.

Index Terms—LGAD, TCAD, SIMS, acceptor degeneration, neutron irradiation, radiation model, breakdown

I. INTRODUCTION

Low Gain Avalanche Detector (LGAD) has been developed extensively in the past few years [1–7] owing to excellent timing performance, mostly driven by the High Luminosity LHC (HL-LHC) upgrade and CERN RD50 Collaboration [8]. It will be used on the ATLAS and the CMS experiments, namely High Granularity Timing Detector (HGTD) [9] and the End-cap Timing Layer (ETL) [10], respectively. The required radiation hardness up to $2.5 \times 10^{15} \text{ n}_{\text{eq}}/\text{cm}^2$ for ATLAS is the main challenge for LGAD sensor. Technology Computer-Aided Design (TCAD) usually be applied to the optimization of semiconductor processing and prediction of device performance through solving partial equations. Once it is possible to predict characteristics of LGAD sensor accurately before and after irradiation that is beneficial to understand the micro mechanism of radiation damage in LGAD sensor.

One of the key design considerations for LGAD sensor is to obtain appropriate gain by optimizing the breakdown voltage (V_{BD}). Using TCAD tools, early device breakdown could be avoided by precisely calibrated simulation. However, previous simulated V_{BD} of LGAD sensor [11, 12] show discrepancies when compared with measurements. Gain layer doping and avalanche model are the major causes of such discrepancies. Therefore, calibrated process simulation with SIMS measurement could minimize the influence of doping

Tao Yang, Kewei Wu, Xuewei Jia, Yuhang Tan, Suyu Xiao, Mengzhao Li, Shuqi Li, Chengjun Yu, Han Cui, Hao Zeng, Mingjie Zhai, Shuiting Xin, Maoqiang Jing are with Institute of High Energy Physics, CAS and University of Chinese Academy of Sciences.

Mei Zhao, Kai Liu, Yunyun Fan, Zhijun Liang, João Guimarães da Costa and Xin Shi, are with Institute of High Energy Physics, CAS (e-mail: shixin@ihep.ac.cn).

Gangping Yan, Qionghua Zhai, Mingzheng Ding, Gaobo Xu and Huaxiang Yin are with Institute of Microelectronics, CAS.

Gregor Kramberger is with the Jozef Stefan Institute, SI-1000 Ljubljana, Slovenia.

uncertainty while configuring appropriate physical models in simulation can predict the threshold of breakdown precisely.

Furthermore, considering a better model to predict the irradiated LGAD sensor by TCAD simulation based on previous phenomenological studies is an important research topic [8]. Previous studies [13, 14] report different models applied in TCAD simulation and give qualitative results for irradiated LGAD sensor without explicit verification. One comprehensive study [15] which simulates the gain factor is verified on irradiated LGAD sensor from different vendors, but the leakage current and capacitance in irradiated LGAD sensor also not be predicted. For this reason, this paper presents a precise TCAD simulation based on IHEP-IME-v1 LGAD sensors and proposes the LRDM to evaluate the leakage current and capacitance of irradiated LGAD sensor.

II. DEVICES UNDER STUDY

IHEP-IME-v1 LGAD sensor is developed by Institute of High Energy Physics and Institute of Microelectronics of the Chinese Academy of Sciences [16]. The cross-section of IHEP-IME-v1 LGAD structure is shown in Fig. 1. Typically, full structure contains (n++)-(p+)-p-(p++) stack, junction termination extension (JTE), p-stop and guard-ring. It is manufactured by 50 μm high resistivity p-type epi-wafer with $\sim 725 \mu\text{m}$ supporting substrate, and detailed information can be found in TABLE I. The electric field peak in p+ gain layer larger than 300 kV/cm when LGAD sensor operates at an appropriate reverse voltage. Under this condition, the drift electrons (a few holes) acquire sufficient energy to generate electron-hole pairs by impact ionization but lower than the avalanche threshold. The gain of LGAD sensor is kept under control at around 10-60 where good time resolution σ_t and signal noise ratio S/N achieve simultaneously due to carriers multiplication and thin active region [17].

To understand the difference between measurements and simulations and to minimize it, we select two fabricated devices of IHEP-IME-v1 production where LGAD (L1-15-100) and PIN (PIN-15-100). Both of them have same geometry and fabricating process except PIN without gain layer (Fig. 2(a) and 2(b)). The active area of them are $1.3 \times 1.3 \text{ mm}^2$. Fig. 3(a) and 3(b) show the I-V and $1/C^2\text{-V}$ of LGAD/PIN measured under room temperature. Owing to internal gain, the leakage current of LGAD sensor is around 2-15 times than PIN between device is full depleted and breakdown. And

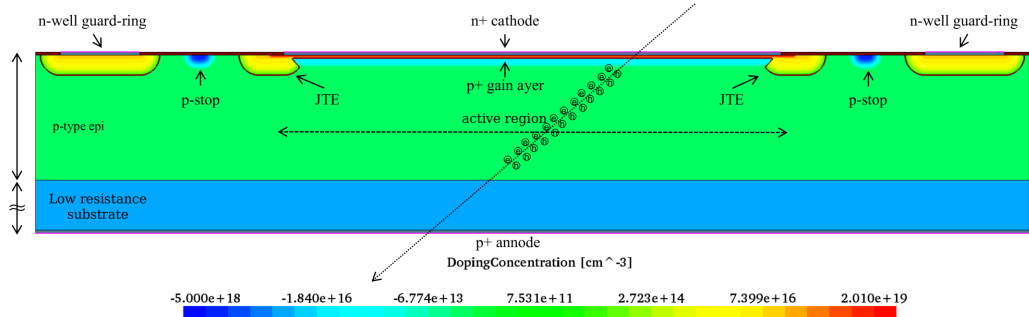


Fig. 1. Schematic cross-section of LGAD with JTE, P-stop and N-well guard-ring. JTE could prevent premature breakdown [2]. Guard-ring is “cathode” for the peripheral region and simultaneously reshapes electric field distribution near the region of JTE. P-stop blocks up the potential connection between cathode and guard-ring considering JTE diffusion process and interface charges after radiation when the same voltage is applied in cathode/guard-ring.

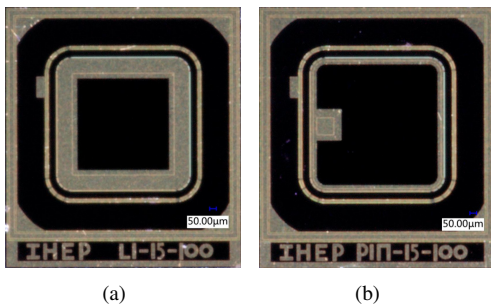


Fig. 2. (a) IHEP-IME-v1 LGAD and (b) PIN devices with same JTE and GR structures.

TABLE I
WAFER SPECIFICATION

	parameter	value
epi	thickness	50 ~ 55 μ m
	uniformity	6%
	dopant	Intrinsic (p-type)
	resistivity	> 1000 $\Omega \cdot \text{cm}$
sub	material	Czochralski silicon
	thickness	725 \pm 20 μ m
	orientation	<100>
	dopant	Boron
	resistivity	< 0.02 $\Omega \cdot \text{cm}$

the V_{BD} of LGAD (~ 196 V) is earlier than PIN (> 700 V) which is determined when leakage current exceeds 10^{-6} A. The gain layer depleted voltage (V_{GL}) before full depleted voltage (V_{FD}) in LGAD sensor corresponds the (n++)-(p+)-(p)-(p++) stack.

Effective doping concentration N_{eff} can be extracted from $d(1/C^2)/dV$ as

$$N_{eff} = \frac{2}{q\epsilon A^2 d(1/C^2)/dV} \quad (1)$$

where q is the electron charge, ϵ is the dielectric constant of silicon and A is the active area of the active region. The effective doping of the bulk region ($N_{BULK} = 9.8 \times 10^{12} \text{ cm}^{-3}$) could be extracted by the slope of $1/C^2$ -V before fully depleted in PIN. The corresponding resistivity is $1355 \Omega \cdot \text{cm}$ that consists with the resistivity of the epitaxial layer provided by the wafer factory in TABLE I. It should be emphasized

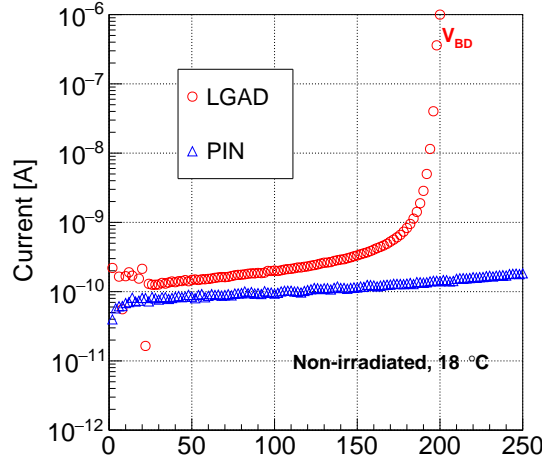
that equation (1) is accurate if the depleted region grows from the main junction side only called “one-sided junction” approximation. The same method could be applied on LGAD, but different n+ diffusion processes, shallow gain layer, and JTE junction extension lead to less accurate determination of doping profile. So the extracted doping profile is a conservative estimation.

III. TCAD SIMULATION

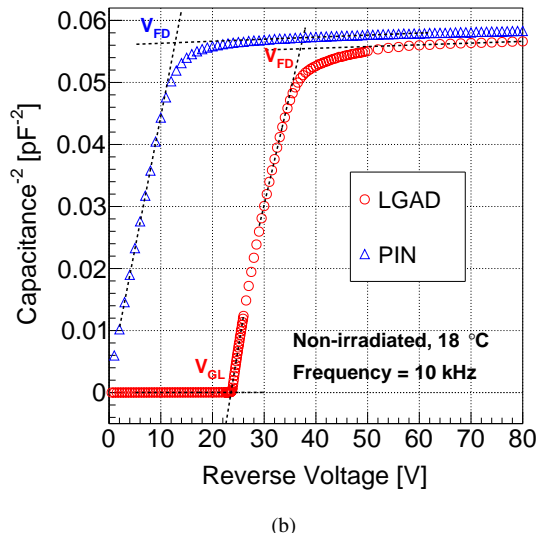
The full TCAD simulation includes device construction and simulation of the electrical properties. The device construction contains the definition of geometry and doping profile. The geometry could be scaled-down to reduce the time budget and the doping profile could be extracted from $1/C^2$ -V or generated by process simulation. For simulation of the electrical properties, the selected physical models are significant for LGAD sensor owing to its particularity in electric field and doping concentration.

A. Doping profile from $1/C^2$ -V

As mentioned in the last section, there are discrepancies between the doping profile from $1/C^2$ -V and the practical doping profile. Fig. 4 shows the measured phosphorus, boron concentration by SIMS and calculated doping (effective doping) by (1), and it indicates there are differences no matter depth or doping level on peak of the gain layer. If implanted phosphorus and boron are totally activated, the difference between SIMS and calculation could be explained by the “one-sided junction” approximation from (1). The dissimilarity of peak position between calculation and SIMS is caused by the metallurgical junction line under surface. And the peak of effective doping difference $N_{eff}(\text{SIMS})/N_{eff}(\text{Cal}) = 1.34$ is from “one-sided approximation” when calculate doping. Though previous studies used the calculated doping to simulate gain factor [18], the discrepancies of doping induced by this method deteriorated the final simulated breakdown voltage (V_{BD}) should not be neglected. Owing to this reason, TCAD process simulation is adopted to acquire an accurate doping profile of LGAD sensor.



(a)



(b)

Fig. 3. (a) I-V and (b) C-V for non-irradiated IHEP-IME-v1 LGAD and PIN devices which measured on 18 ± 2 °C, 45% humidity environment. The V_{GL} and V_{FD} of LGAD are acquired by two linear functions fitting.

B. Process calibration by SIMS

The process simulation needs to be calibrated by SIMS data before the simulation of electrical characteristics. Synopsys TCAD process simulation provides accurate ion implantation database called “Advanced Calibration” [19], but there are large discrepancies between process simulation by “Advanced Calibration” and SIMS (Fig. 5(a) and 5(b)). For phosphorus, the simulated doping is shallower than SIMS. For boron, another bump on the tail which indicates the channeling effects is overestimated in simulation. This phenomenon is caused by oxide layer on the surface (cap-layer) implemented during ion implantation. The layer prevents the channeling effects. In the actual fabricated process, there is a thin oxide shield layer(~ 120 nm) covering on wafer surface (pre-amorphization) to suppress channeling effects. However, one

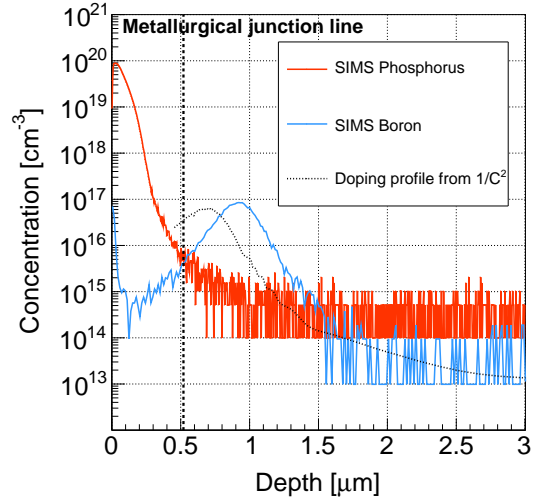


Fig. 4. (Color online) SIMS results for IHEP-IME-v1 LGAD sensor: phosphorus(red line) and boron(blue line). calculated effective doping from $1/C^2$ -V is dashed line. The detection limit of SIMS technology: phosphorus $\sim 10^{15}$ atom/cm 3 , boron $\sim 10^{14}$ atom/cm 3 .

thermal oxide layer has been added before implantation, the channeling effects still are not suppressed as expected in simulation. To calibrate ion implantation step in simulation, “Cap Layer-Dependent” parameter r [19] should be corrected.

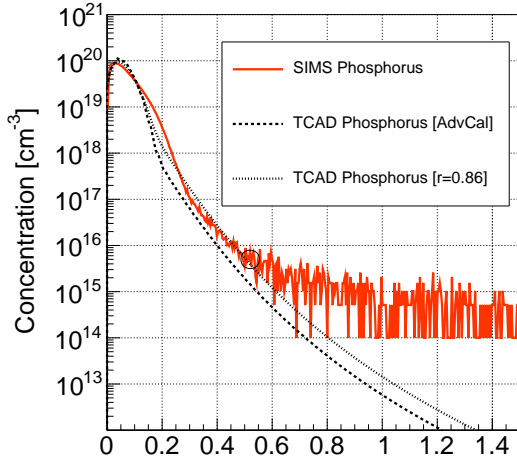
For a calibration driven by data, the ratio of “channeling effects suppression” are adjusted for both phosphorus and boron: $r_{boron} = 0.99$ and $r_{phosphorus} = 0.86$ to minimize $(N_{TCAD} - N_{SIMS})^2$. After calibration, the simulated doping profiles have good agreement with SIMS data.

C. configuration of physical model

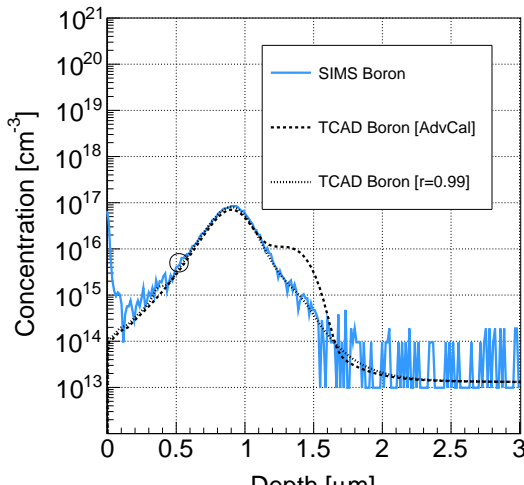
Considering the effective doping larger than 10^{16} cm $^{-3}$, the electric field on gain layer around 3×10^5 V/cm and low-temperature condition, more physical effects need to be added in simulation. The applied physical models list in below: “DopingDependence” and “HighFieldSaturation” on mobility; “DopingDependence” and “TempDependence” on Shockley–Read–Hall Recombination (SRH). The avalanche model use van Overstraeten – de Man model [20] with “Eparallel” driving force. For van Overstraeten – de Man model, the electric field on 1.75×10^5 V/cm to 4×10^5 V/cm and $> 4 \times 10^5$ V/cm have two sets of parameters for carrier generation coefficient that determines the breakdown threshold of LGAD sensor.

D. Simulated I-V & C-V for non-irradiated LGAD sensor

We use the PIN and LGAD to verify our simulation setup based on the calibrated process simulation and applied physical model. Several devices are measured to estimate the spread of IV for produced devices, which can be due to fabrication non-uniformity as well as measurement conditions (color band in Fig. 6(a)). The simulated current agrees with measurements well, especially predicts the breakdown voltage of LGAD sensors accurately. The bias region from V_{FD} to



(a)



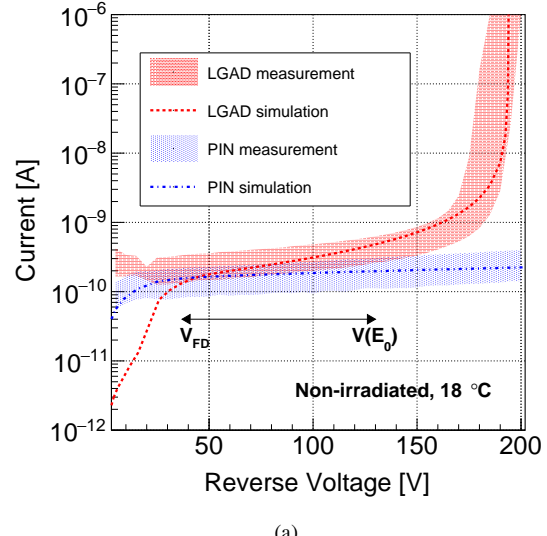
(b)

Fig. 5. (Color online) (a) phosphorus and (b) born distribution before and after calibration. The simulated doping profiles consist with SIMS results by adjusting the “Cap Layer-Dependent” parameter r . There is huge distortion between the simulated doping profiles by “AdvancedCalibration” and SIMS results. The circle marks the position of the metallurgical junction line.

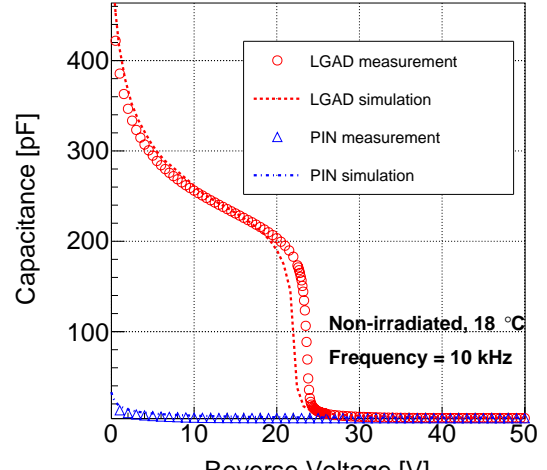
$V(E_0 = 4 \times 10^5 \text{ V/cm})$, denoted by the arrow in Fig. 8 is the operation region with moderate gain. The predicted breakdown voltage agrees with Overstraeten models. Fig. 7 is electric field peak on the gain layer, which is simulated by TCAD using calibrated processing in Section III-B. When the electric field exceeds the threshold E_0 , sharp increase in leakage current due to high field generation.

The simulated capacitances show in Fig. 6(b), and they also agree well with measurements. The remained discrepancies originate from the assumed symmetry in simulations (2D simulation), which for fabricated devices is not perfect.

We compare 4 different process sets simulated and measured I-V of LGAD sensors after calibration (Fig. 8) to verify the reliability of the simulation setup, and the same simulation



(a)



(b)

Fig. 6. (Color online) (a) I-V and (b) C-V for LGAD and PIN. The color band of measured I-V is from several LGAD devices which have same structure and fabricated process.

TABLE II
LGAD PROCESS SET

Phosphorus		Low	Energy	High	Energy
Boron		(1.00)		(1.25)	
Low Dose (1.00)		set2		set1	
High Dose (1.14)		set4		set3	

setup is applied for all process sets. The process sets list in TABLE II, the selected LGAD sensor in Section II is fabricated by set3. After using the same simulation setup, all simulated breakdown voltages show good consistency with measurements. It proves the calibrated configurations in the process simulation are successful and V_{BD} could be predicted by applied physical models.

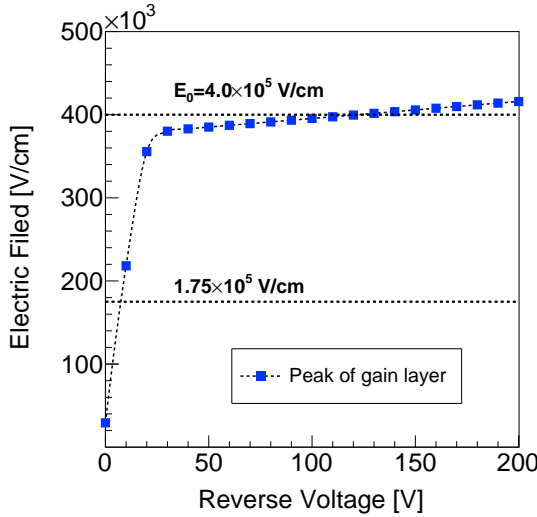


Fig. 7. Simulated electric field peak on gain layer. Additional 2 dash lines mark $1.75 \times 10^5 \text{ V/cm}$ and $4 \times 10^5 \text{ V/cm}$ electric field threshold for van Overstraeten model.

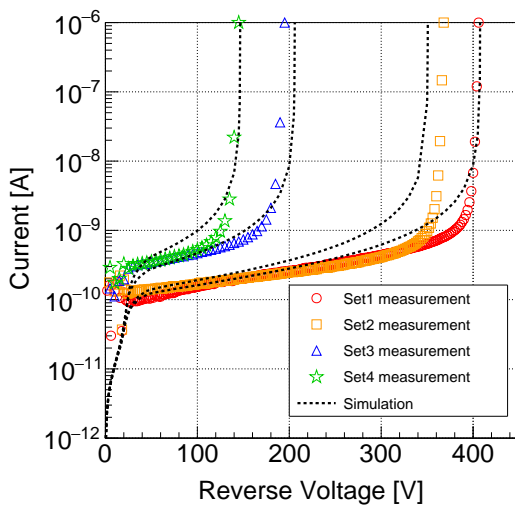


Fig. 8. Leakage current for simulation (dashed line) and measurement for 4 different process sets after calibration. The details of 4 process sets see TABLE II.

IV. RADIATION MODEL

A. LGAD Radiation Damage Model (LRDM)

We propose the LRDM which combines local acceptor degeneration with global deep energy levels in TCAD simulation to predict the current and capacitance for irradiated LGAD sensor. The acceptor degeneration only takes effect in the gain layer and the deep energy levels are implemented in the high resistivity bulk region. Equation (2) is the Poisson equation that separates acceptor degeneration and deep energy levels in different regions.

$$-\nabla \cdot (\epsilon \nabla \phi) = q(p - n - \{N_A^{\text{eff}}\}_{\text{gain}}) + \{q \sum_i N_{ti}(\delta_i - f_{ti})\}_{\text{bulk}} \quad (2)$$

where N_{ti} is trap concentration, $\delta_i = 1$ (or 0) for donor (or acceptor) type trap and f_{ti} is trap occupancy for trap i .

For the acceptor degeneration model, consider the theoretical prediction of the effective doping N_A^{eff} after irradiation [21]:

$$N_A^{\text{eff}}(\Phi_{\text{eq}}) = N_A(0) + g\Phi_{\text{eq}} - N_A(0)[1 - \exp(-c\Phi_{\text{eq}})] \quad (3)$$

where Φ_{eq} is equivalent to 1 MeV neutron fluence by NIEL hypothesis, $N_A(0)$ and $N_A^{\text{eff}}(0)$ are initial and effective doping when non-irradiated. we set the degeneration constant $c = 3.23 \times 10^{-16} \text{ cm}^2$ and $g = 0.02 \text{ cm}^{-1}$ [22].

For the deep energy levels model, Hamburg Penta Trap Model (HPTM) [23] is applied, owing to HPTM gives a consistent description of a large set of measurements in PIN with protons fluence range from 3×10^{14} to $1.3 \times 10^{16} \text{ n}_{\text{eq}}/\text{cm}^2$ under low temperature. The 5 deep energy levels of HPTM are implemented in silicon material with uniform distribution in TCAD simulation.

B. Simulated I-V and C-V for irradiated LGAD sensor

Once we confirm our simulation setup and implement the LRDM, equations (2) and current continuity equations could be solved in order to estimate the leakage current and capacitance for irradiated LGAD sensor. The studied LGAD sensor is irradiated at the Jozef Stefan Institute (JSI) with $2.5 \times 10^{15} \text{ n}_{\text{eq}}/\text{cm}^2$. The measurements of irradiated LGAD sensor are performed after 80 min@60 °C annealing.

The leakage current of irradiated LGAD sensor has two contributing parts: residual gain and deep energy traps. It is determined by [24]:

$$I(\Phi_{\text{eq}}) = M_I(\Phi_{\text{eq}}) \times I_{\text{gen}}(\Phi_{\text{eq}}) \quad (4)$$

where $M_I(\Phi_{\text{eq}})$ is dominated by acceptor degeneration and $I_{\text{gen}}(\Phi_{\text{eq}})$ by deep energy levels. The simulated current for $\Phi_{\text{eq}} = 2.5 \times 10^{15} \text{ n}_{\text{eq}}/\text{cm}^2$ shows in Fig. 9. The simulated result predicts the large increase of leakage current and V_{BD} in irradiated LGAD sensor which consists of measurements. The discrepancies of leakage current level between simulation and measurement are from the following contributions: the uncertainty of irradiation fluence, electric field fluctuation caused by HPTM model, imperfect applicability of HPTM model in LGAD sensor, the distortion of avalanche model at low temperature. We find the leading contributing deep level of HPTM is I_p with the introduction rate $g_{\text{int}}(I_p) = 0.4335$ (default HPTM value) and the deep level concentration $N(I_p) = g_{\text{int}}(I_p) \times \Phi_{\text{eq}}$. The optimization of $g_{\text{int}}(I_p) = 0.6050$ with acceptor degeneration could fix the discrepancies at high reverse voltage.

The Fig. 10 reflects another significant prediction of the LRDM - the valley in $1/C^2$ -V of irradiated LGAD sensor at low temperature, 1 kHz frequency when gain layer depleted. This phenomenon has been reported in previous works for irradiated CNM LGAD sensors [25]. And extensive measurements [22, 26] for irradiated LGAD sensors under room temperature

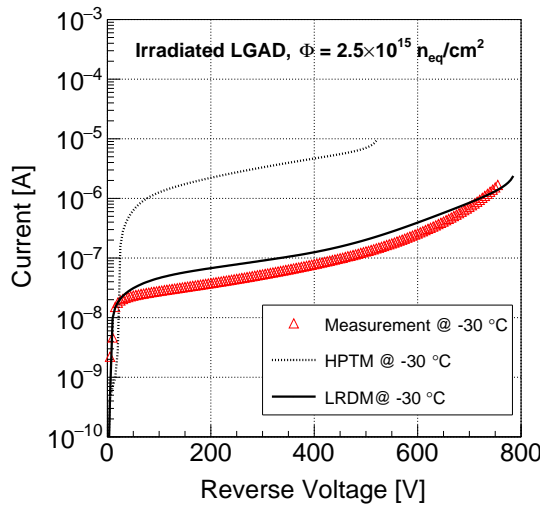


Fig. 9. Leakage current of simulation (dashed and solid) and measurement (triangle) for $\Phi_{eq} = 2.5 \times 10^{15} n_{eq}/cm^2$ @-30 °C. The LRDM is implemented in TCAD @-30 °C. The solid line is enhanced the $g_{int}(I_p)$ from 0.4335 (default HPTM value) to 0.6050 with acceptor degeneration model.

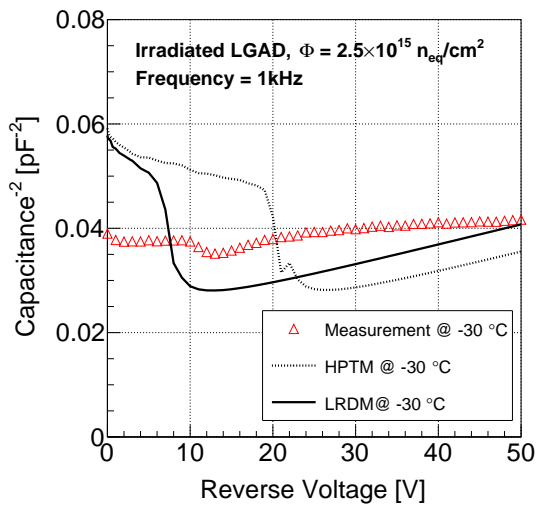


Fig. 10. Capacitance of simulation (dashed and solid) and measurement (triangle @-30 °C, circle at room temperature ~18 °C) for $\Phi_{eq} = 2.5 \times 10^{15} n_{eq}/cm^2$. The LRDM is implemented in TCAD @-30 °C. The solid line is enhanced the $g_{int}(I_p)$ from 0.4335 (default HPTM value) to 0.6050 with acceptor degeneration model.

indicate this valley only stands out at low temperature. Similarly, the optimizing $g_{int}(I_p) = 0.6050$ could suppress the discrepancies after gain layer depleted ($V_{GL} = 10.5$) with a higher introduction rate of I_p level. However, the theoretical interpretation about the behaviors of LGAD capacitance at low temperature lacks at present and there are still large discrepancies between simulation and measurement before V_{GL} . Further study would be continued in the future.

V. SUMMARY

This paper presents a precise process simulation after calibration for the first production IHEP-IME LGAD sensor and

the simulation setup is verified by the various process. With SIMS technology, the channeling suppression is considered in process simulation which agrees with data. Highly consistent characteristics in non-irradiated LGAD sensors benefit to the precise optimization for IHEP-IME-v2 production and lay a foundation for the simulation of irradiated LGAD sensors.

The LRDM which combines local acceptor degeneration and global deep energy levels is proposed to simulate the characteristics of irradiated LGAD sensor. The simulated leakage current agrees well with the measurements. Meanwhile, the simulated capacitance by LRDM reproduce the valley in $1/C^2-V$ at -30 °C. Further study about the radiation model and theoretical explanation about behaviors of capacitance in irradiated LGAD sensor need more measurements supporting by other technologies. The deep energy levels in irradiated LGAD could be extracted by Thermally Stimulated Current (TSC) [27] and the electric field distribution could be acquired by edge -Transit Current Technique (e-TCT) [28] and Two-Photon Absorption - Transient Current Technique (TPA-TCT) [29].

ACKNOWLEDGMENT

This work is supported by the National Natural Science Foundation of China (No. 11961141014), the Scientific Instrument Developing Project of the Chinese Academy of Sciences - Grant (No. ZDKYYQ20200007) and the National Key Research & Development Program (No. 2016YFA0201903). We recognize the key suggestions from ATLAS HGTD Collaboration and CERN RD50 Collaboration. Thanks for Joern Schwandt's comments about the radiation model in TCAD simulation.

REFERENCES

- [1] G. Pellegrini *et al.*, “Technology developments and first measurements of Low Gain Avalanche Detectors (LGAD) for high energy physics applications,” *Nucl. Instrum. Methods A*, vol. 765, 2014.
- [2] H. F. W. Sadrozinski *et al.*, “4D tracking with ultra-fast silicon detectors,” *Rep. Prog. Phys.*, vol. 81, no. 2, 2018.
- [3] V. Sola *et al.*, “First FBK production of 50 um ultra-fast silicon detectors,” *Nucl. Instrum. Methods A*, vol. 924, 2019, 11th International Hiroshima Symposium on Development and Application of Semiconductor Tracking Detectors.
- [4] Y. Fan *et al.*, “Radiation hardness of the low gain avalanche diodes developed by NDL and IHEP in China,” *Nucl. Instrum. Methods A*, vol. 984, 2020.
- [5] S. Xiao *et al.*, “Beam test results of NDL Low Gain Avalanche Detectors (LGAD),” *Nucl. Instrum. Methods A*, vol. 989, 2021.
- [6] Y. Tan *et al.*, “Radiation effects on NDL prototype LGAD sensors after proton irradiation,” *Nucl. Instrum. Methods A*, vol. 1010, 2021.
- [7] G. Giacomini *et al.*, “Development of a technology for the fabrication of low-gain avalanche diodes at bnl,” *Nucl. Instrum. Methods A*, vol. 934, 2019.
- [8] RD50 Collaboration, “RD50 prolongation request 2018.”

[9] ATLAS Collaboration, “Technical Proposal: A High-Granularity Timing Detector for the ATLAS Phase-II Upgrade,” Tech. Rep. CERN-LHCC-2018-023. LHCC-P-012, 2018.

[10] CMS Collaboration, “A MIP Timing Detector for the CMS Phase-2 Upgrade,” Tech. Rep. CERN-LHCC-2019-003. CMS-TDR-020, 2019.

[11] N. Moffat *et al.*, “Low Gain Avalanche Detectors (LGAD) for particle physics and synchrotron applications,” *Journal of Instrumentation*, vol. 13, no. 03, 2018.

[12] D. Flores *et al.*, “Optimization and Fabrication of LGAD Detectors with the aid of TCAD Simulations,” 2016, 2nd SIMDET.

[13] R. Dalal *et al.*, “TCAD simulation of Low Gain Avalanche Detectors,” *Nucl. Instrum. Methods A*, vol. 836, 2016.

[14] F. Palomo *et al.*, “TCAD and recent defect studies,” 2019, The 28th International Workshop on Vertex Detectors.

[15] M. Mandurrino *et al.*, “Analysis and numerical design of Resistive AC-Coupled Silicon Detectors (RSD) for 4D particle tracking,” *Nucl. Instrum. Methods A*, vol. 959, 2020.

[16] K. Wu *et al.*, “Design of Low Gain Avalanche Detectors (LGAD) with 400 keV ion implantation energy for multiplication layer fabrication,” *Nucl. Instrum. Methods A*, vol. 984, 2020.

[17] V. Sola *et al.*, “Ultra-Fast Silicon Detectors for 4D tracking,” *Journal of Instrumentation*, vol. 12, no. 02, 2017.

[18] Z. Galloway *et al.*, “Properties of HPK UFSD after neutron irradiation up to $6e15$ n/cm 2 ,” *Nucl. Instrum. Methods A*, vol. 940, 2019.

[19] “Sentaurus manual.” [Online]. Available: <https://www.synopsys.com/>

[20] R. Van Overstraeten *et al.*, “Measurement of the ionization rates in diffused silicon p-n junctions,” *Solid-State Electronics*, vol. 13, no. 5, 1970.

[21] M. Moll, “Radiation induced performance degradation of p-type silicon devices by acceptor removal effects,” 2019, The 28th International Workshop on Vertex Detectors.

[22] M. Ferrero *et al.*, “Radiation resistant lgad design,” *Nucl. Instrum. Methods A*, vol. 919, 2019.

[23] J. Schwandt *et al.*, “A new model for the TCAD simulation of the silicon damage by high fluence proton irradiation,” 2019.

[24] G. Kramberger *et al.*, “Radiation hardness of thin Low Gain Avalanche Detectors,” *Nucl. Instrum. Methods A*, vol. 891, 2018.

[25] S. Otero Ugobono *et al.*, “Radiation Tolerance of Proton-Irradiated LGADs,” *IEEE Transactions on Nuclear Science*, vol. 65, no. 8, 2018.

[26] R. Padilla *et al.*, “Effect of deep gain layer and Carbon infusion on LGAD radiation hardness,” *Journal of Instrumentation*, vol. 15, no. 10, 2020.

[27] I. Pintilie, “Defect investigations of neutron irradiated high resistivity PiN and LGAD diodes,” 2019, The 35th RD50 Workshop.

[28] M. Wiehe *et al.*, “Study of the radiation-induced damage mechanism in proton irradiated low gain avalanche detectors and its thermal annealing dependence,” *Nucl. Instrum. Methods A*, vol. 986, 2021.

[29] S. Otero Ugobono *et al.*, in *Proceedings of The 26th International Workshop on Vertex Detectors — PoS(Vertex 2017)*, vol. 309, 2018.